

Non-equilibrium heating path for ultrafast laser-induced nucleation of skyrmion lattices.

P. Olleros-Rodríguez,^{1,*} M. Strungaru,^{2,†} S. Ruta,² P. Gavriloea,²
P. Perna,^{1,‡} R. W Chantrell,^{2,§} and O. Chubykalo-Fesenko^{3,¶}

¹*IMDEA Nanociencia, Campus de Cantoblanco, 28049 Madrid, Spain.*

²*Department of Physics, University of York, YO10 5DD, York, United Kingdom*

³*Materials Science Institute ICMM-CSIC, Campus de Cantoblanco, 28049, Madrid, Spain.*

(Dated: May 20, 2022)

We explore the helicity-independent light-induced nucleation of skyrmion lattices in ferromagnetic cobalt-based trilayers with perpendicular magnetic anisotropy. Using Atomistic Spin Dynamics simulations, we show that a high temperature excitation followed by magnon drops and their non-equilibrium relaxation, accessed by an ultrafast laser excitation with specific duration and intensity, can lead to the generation of a skyrmion lattice stable at room-temperature. The nucleation window, the topological density and the skyrmion polarity can be additionally manipulated by external magnetic fields. Our results provide insight into the non-equilibrium nature of skyrmionic excitations at non-zero temperatures and pave additional routes for their use in information technologies.

Magnetic Skyrmions (Sk) are nanometer sized topologically protected spin-textures appearing in magnetic systems that exhibit Dzyaloshinskii-Moriya interaction(DMI)[1, 2]. Due to their reduced sizes and transport properties via spin-polarised currents, magnetic skyrmions are considered promising candidates as information carriers in next-generation spintronic devices [3–6] or novel reservoir and neuromorphic computing [7, 8]. Among several possibilities, skyrmions in thin multilayers composed of transition metals and high spin-orbit coupling materials [3, 6, 9] are especially interesting due to the potential usage at room temperature (RT) and long-time thermal stability. The use of skyrmions in technological applications is constrained by the necessity to nucleate them with controlled polarization. Since in thin film multilayers small Neel skyrmions in the absence of an external field are typically metastable structures, this frequently requires special protocols such as bipolar current pulse trains [10], current injection through nanocontacts [6] or specially designed patterned constrictions and injectors [11, 12].

Recently, research on optically induced ultrafast magnetisation dynamics triggered by femtosecond laser pulses in ferro- and ferrimagnetic materials is gaining considerable interest given its localised and ultrafast character[13]. In this scenario, magnetisation dynamics can be induced due to purely thermal magnetic excitations by ultrafast heat produced by a linearly polarised laser pulse [14]. Particularly, it has been shown that skyrmions or bubbles can be nucleated by applying laser pulses [15, 16]. The skyrmions densities and sizes were reported to depend on the laser parameters. Since intrinsic characteristics of skyrmions only rely on the material properties, these dependencies can be explained by thermal magnetisation reversal in a large region under the laser spot stabilised by magnetostatic interactions giving rise to large magnetic bubbles [15].

In the present Letter, using atomistic spin dynam-

ics (ASD) modelling we demonstrate the efficient generation of small skyrmions (with diameters below 20 nm) in realistically parametrised Pt/Co(3ML)/Heavy-metal(HM) magnetic trilayers [17, 18] under the effect of non-equilibrium temperature dynamics produced by a femtosecond laser excitation. It has been shown that Co layers sandwiched between different heavy metals exhibit a strong DMI [9, 18, 19] that leads to stabilisation of small skyrmions. Moreover, the large and tunable perpendicular magnetic anisotropy (PMA) of Co-based systems and the topological protection of these nanostructures can benefit their thermal stability. ASD models have been demonstrated to be a powerful technique in studying laser-induced magnetization dynamics [14, 20, 21], concerning especially a rapid heating to temperatures above the Curie temperature (T_C). In this Letter we show that a slow cooling from paramagnetic state creates a stripe-domain configuration in our modelled system. At the same time for a set of specific laser-pulse parameters it is possible to nucleate skyrmions in the absence of magnetic fields due to the highly non-equilibrium excitation and relaxation path of magnon drops. Furthermore, we demonstrate that the skyrmion density can be manipulated by the laser properties and external magnetic fields.

The ASD simulations were performed using the software package VAMPIRE [22]. The spin Hamiltonian, consisting of the Heisenberg exchange, anisotropy, Zeeman and DMI energies, is written as:

$$\begin{aligned} \mathcal{H}_{spin} = & - \sum_{i<j} J_{ij} (\mathbf{S}_i \cdot \mathbf{S}_j) - K_u \sum_i (\mathbf{S}_i \cdot \hat{\mathbf{e}})^2 - \\ & - \mu_S \sum_i (\mathbf{S}_i \cdot \mathbf{B}_{app}) - \sum_{i<j} \mathbf{D}_{ij} \cdot (\mathbf{S}_i \times \mathbf{S}_j) \end{aligned} \quad (1)$$

where \mathbf{S}_i and \mathbf{S}_j are unit vectors referring to the spin in the sites i and j respectively. J_{ij} is the symmetric exchange interaction between spins i and j , K_u is the uniaxial anisotropy of the system with the easy axis

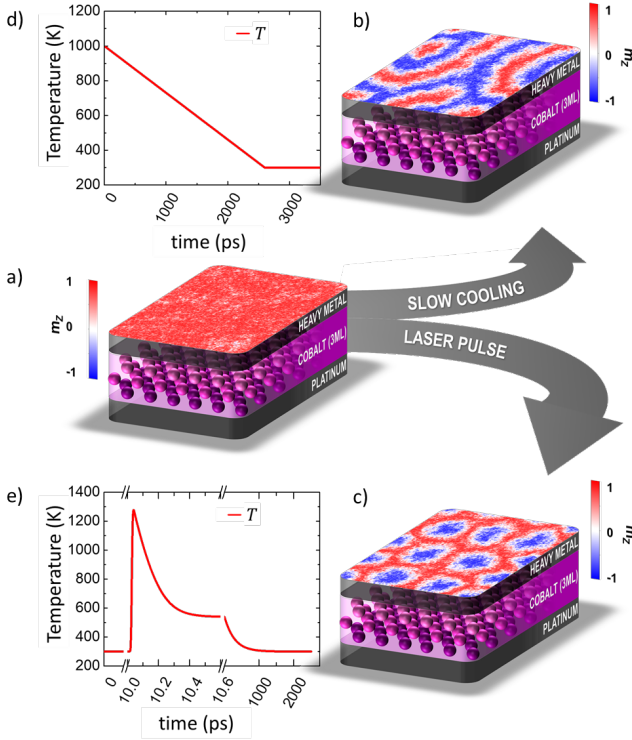


FIG. 1. (Color online) **Illustration of the nucleation protocols.** a) Sketch of the Pt/Co(3ML)/HM system modelled by using the parameters listed in Table 1. The top layer presents the initial spin configuration; b) Ground state obtained after slow cooling (temperature profile presented in d)) from a paramagnetic state (above system's $T_C = 754.29$ K) to the room temperature following a quasi-equilibrium dynamical path. c) Skyrmion lattice obtained when a laser-pulse is applied to the system (fluence $F_0 = 5.6 \text{ mJ/cm}^2$ and pulse-length of 10 fs); The electron temperature profile is presented in panel e). The final temperature of both systems is $T_f = 300 \text{ K}$.

pointing along the direction defined by the unit vector \hat{e} , μ_S is the magnetic moment of the spin, \mathbf{B}_{app} is the external applied field and \mathbf{D}_{ij} is the DMI vector calculated as $\mathbf{D}_{ij} = D(\mathbf{z} \times \mathbf{r}_{ij})$ [18], with \mathbf{z} and \mathbf{r}_{ij} being the unit vectors that point along z direction and the relative distance between atoms i and j respectively. The modelled system consists of 3 monolayers (3ML) of hexagonal closed-packed Cobalt. The sample is parametrised using the uniaxial perpendicular anisotropy and exchange energy corresponding to bulk Co [17]. The DMI interaction for a Pt/Co interface is parametrised from first principles calculations [18] and matches that obtained experimentally [23, 24] and calculated in the micromagnetic approximation [25]. The parameters used in the simulation are given in Table I. The magnetisation dynamics is obtained by solving the set of atomistic stochastic Landau-Lifshitz-Gilbert (LLG) equations coupled to the electronic temperature $T_e(t)$. The effect of the laser pulse is included by the Two-Temperature Model (2TM)[26] for coupled

TABLE I. **Magnetic and 2TM parameters used for modelling Co trilayers.**

Magnetic parameters (Co)	
Exchange energy, J_{ij}	$4.8 \times 10^{-21} \text{ J/atom}$ ^(a)
DMI energy, D	$4.8 \times 10^{-22} \text{ J/atom}$ ^(a)
Uniaxial Anisotropy, K_u	$5.85 \times 10^{-24} \text{ J/atom}$ ^(b)
Damping, α	0.3 ^(c)
2TM parameters	
Electron specific heat parameter, γ_{sp}	$662 \text{ J/m}^3 \text{ K}^2$ ^(d)
Phonon specific heat, C_l	$2.07 \times 10^6 \text{ J/(m}^3 \text{ K)}$ ^(d)
Electron-phonon coupling, G_{el}	$4.05 \times 10^{18} \text{ J/(sm}^3 \text{ K)}$ ^(d)
Heat-sink coupling, κ_e	$4 \times 10^9 \text{ s}^{-1}$ ^(e)

^(a) Reference [18]

^(b) Reference [17]

^(c) Reference [27]

^(d) Reference [28]

^(e) Reference [29]

electronic (T_e) and lattice (T_l) temperatures dynamics excited by a laser pulse of a power density $P(t)$:

$$\begin{aligned}
 C_e \frac{\partial T_e}{\partial t} &= -G_{el}(T_e - T_l) + P(t) \\
 C_l \frac{\partial T_l}{\partial t} &= G_{el}(T_e - T_l) - \kappa_e \nabla T_l
 \end{aligned} \tag{2}$$

where $C_e = \gamma_{sp} \cdot T_e$ is the electronic specific heat, C_l is the lattice specific heat, G_{el} the electron-phonon coupling and κ_e the diffusion coefficient representing the heat dissipation to the environment. The laser power density is considered with a Gaussian form $P(t) = [2F_0/(\delta t_p \sqrt{\pi/\ln 2})] \cdot \exp[-(4\ln 2)(\frac{t}{t_p})^2]$ where F_0 is the laser fluence (in units of energy density), t_p the pulse temporal width and δ the optical penetration depth, assumed to be $\delta = 10 \text{ nm}$. Note that the deposited energy is independent of the pulse width for a given laser fluence. The 2TM parameters used in the simulation are given in Table I.

Fig.1 illustrates the nucleation protocols used in this work for skyrmion generation in zero external field; Panel a) shows schematically the modelled Co-based trilayer. Following a quasi-equilibrium dynamical path, i.e., a slow cooling process from temperature $T > T_C$ (See Suppl. Mat.) to RT as indicated in Fig.1d, the final magnetic configuration (the ground state) consists of labyrinthine domains (Fig.1b) as typically obtained in systems with PMA. On the contrary, starting from a saturated state (Fig.1a) the application of a laser pulse, shown in Fig.1e excites highly non-equilibrium electronic states (leading to a non-equilibrium spin dynamics) which is responsible for the nucleation of a skyrmion lattice shown in panel c). Note that although in both cases the final temperature of the systems is RT, the nucleation of skyrmions is only achieved with ultrafast temperature dynamics resulting from the application of femtosecond laser pulse, proving

that skyrmion lattice is a metastable configuration and that non-equilibrium dynamical path is responsible for its generation. This is different from modelling results of Ref.[30, 31] where skyrmions were a ground state created due to a phase transition from ferromagnetic to the paramagnetic state and consequent cooling in which case there is no necessity for specific ultrafast non-equilibrium excitation.

To quantify the topology of the structures created by the laser pulse, we evaluate the total topological charge Q of the simulated system. In the continuous approach this is given by: $Q = \frac{1}{4\pi} \int \mathbf{S}(\delta_x \mathbf{S} \times \delta_y \mathbf{S}) dx dy$. For a discrete lattice, the topological charge is calculated as in [32], based on the sum of spherical areas given by sets of 3 neighbouring spins placed in a triangle. For a skyrmion lattice with a well-defined chirality of the domain walls and a unique skyrmion polarization $P_{Core} = \pm 1$, the total topological charge of the system characterizes the number of nucleated skyrmions N_{Sk} , i.e. $Q = N_{Sk} \cdot P_{Core}$. For the numerical characterisation of the nucleated skyrmion lattices, independent on the simulated system size, we compute the topological charge surface density.

In our simulations we start from an initial saturated state with the magnetisation pointing along the out-of-plane (OOP) direction (as indicated in Fig.1a) and equilibrate the system at RT ($T = 300$ K). Then, we apply a non-polarised laser pulse of fluence F_0 and temporal width t_p . Fig.2 shows the temperature profile (Panel a) and the magnetisation dynamics (Panel b) following the application of a laser pulse of $t_p = 50$ fs and $F_0 = 6$ mJ/m². Panels c-f) represent the spin configuration of the system at selected times during the process. After equilibrating the system for 10 ps (Region I, left white area in Fig.2b) the laser pulse is applied, leading to an increased electronic temperature. The highly excited electrons change the spin thermal reservoir driving the system to quasi-demagnetised state (Region II, yellow area in Fig.2b). Eventually a mutual thermalisation between the electronic, lattice and spin subsystems takes place on the timescale of hundreds of femtoseconds (Region III, grey area in Fig.2b). Finally, in Region IV (green area) and V (extreme right white region), the heat diffusion dissipates the deposited energy outside the system leading to its thermalisation at RT.

Similarly to the multi-scale domain nucleation processes in ferrimagnetic alloys described in [21], we can separate the ultrafast dynamics and the subsequent skyrmion lattice formation in 2 stages. First, the laser pulse rapidly quenches the magnetisation (see Fig.2c). However, as was pointed out in models of ultrafast magnetisation dynamics[20, 33], the spin correlations are not destroyed. During the so-called *magnon localisation* process (Region III, grey in Fig.2b, and Fig.2d) the recovery of the ferromagnetic order takes place in localised areas of the system due to the short-range atomic exchange

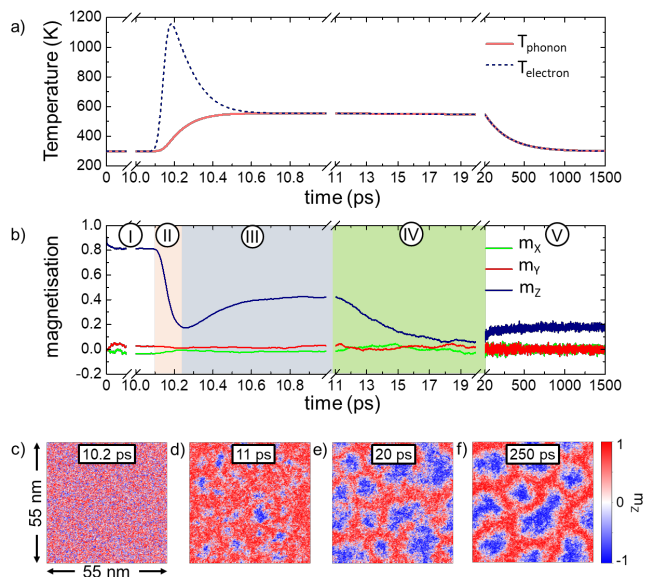


FIG. 2. (Color online) **Laser-induced magnetisation dynamics.** Panel a) Phonon (red solid line) and electron (blue dashed line) temperature dynamics during the simulated light induced nucleation of skyrmion lattices (laser fluence $F_0 = 6$ mJ/m² and a pulse width $t_p = 50$ fs). Panel b) Dynamics of magnetisation components during the light induced nucleation of skyrmion lattice. It can be separated in five regions of interest: (I) Thermal equilibration of the initial OOP saturated state. (II) Demagnetisation process induced by the increase of the electronic (spin) subsystem. (III) Remagnetisation and nucleation of *magnon drops*. (IV) Growth and stabilisation of the magnon drops during the *magnon coalescence*. (V) Room-temperature thermalisation of the system. Panels c-d) OOP-Spin configurations of the 55nm² simulated thin film at selected times (c) $t = 10.2$ ps; demagnetized state (d) $t = 11$ ps; the MDs localisation (e) $t = 20$ ps; magnon coalescence (f) $t = 250$ ps; the skyrmion lattice stabilisation.

interactions. This process leads to the nucleation of unstable and localised spin textures, namely *magnon drops* (MD) [34], following a non-equilibrium path in the spin configuration space. After a time-scale of hundreds of femtoseconds, during the so-called *magnon coalescence* process (Region IV, green in Fig.2b, and Fig.2e) MD can scatter, split or merge until some equilibrium configuration is achieved[35]. Relaxing the spin system to RT by a heat-sink coupling (Region V in Fig.2b), which occurs at the ns timescale, little change in the spin dynamics is observed and the skyrmion structures remain stable versus thermal fluctuations at RT (Fig.2f).

It is worth to emphasise that the magnetisation dynamics leading to the generation of skyrmion lattices takes place in a time scale of picoseconds, following a rapid temperature change in the timescale of the order of 10 ps and below, i.e. it is a highly thermodynamically non-equilibrium path. Instead, slow temperature variations as the one used in Fig.1d and 1b with zero-field

cooling from a temperature above $T_C=754.29\text{K}$ (see more results in Supp. Mat.) in a time scale of few nanoseconds always lead to a complex stripe domain-like configuration. This behaviour unveils the crucial role of the ultrafast character of the laser-induced nucleation of skyrmion lattices.

To find the optimum conditions for the nucleation of skyrmion lattices, we have computed the phase diagram of the topological charge density q as function of laser-pulse width t_p and fluence F_0 in the absence (Fig.3) and presence (Fig.4) of a magnetic external field. This is computed at a short time (250 ps) after the laser pulse is applied, but when all three subsystems (electrons, phonons and spins) are in mutual equilibrium, i.e. have the same temperature. To neglect the effect of a subsequent slow thermal relaxation, a vanishing heat-sink coupling (i.e. $\kappa_e=0$) is considered. Due to the stochastic nature of the dynamics in the presence of temperature, the computed phase diagrams were averaged over 10 random realisations. It is important to note that the skyrmions can nucleate either with their core pointing parallel (P-Sk), i.e. $q > 0$, or antiparallel (AP-Sk) i.e. $q < 0$ to the initial magnetisation direction.

Fig.3 shows the nucleation results in zero external field. The diagram indicates that the skyrmion nucleation takes place for short pulse durations (below 100fs) and in a window of fluences around $F_0 = 6\text{mJ}/\text{cm}^2$. Fig.3c shows the topological charge density dependence on the laser fluence for selected laser pulse lengths (corresponding to the horizontal lines in Fig.3a). It can be observed that $|q|$ increases initially with the fluence, showing a maximum at a fluence of about $6\text{mJ}/\text{cm}^2$, which corresponds to 8 skyrmions generated in the simulated area (see Fig.3f). By analysing the spin configurations, a well defined skyrmion lattice can be obtained with a minimum topological density of $|q| \simeq 1.9 \times 10^{15}\text{m}^{-2}$. This value is considered here as a criterion for the nucleation of a skyrmion lattice. For smaller values of $|q|$, labyrinthic domains coexisting with skyrmions are obtained. A closer inspection of the magnetisation dynamics reveals that the successful nucleation of skyrmion lattices depends on two aspects: i) it is necessary to populate the sample with a sufficiently large number of MDs during the magnon localisation; ii) once the MDs are nucleated, they should gain topological protection so their merging is impeded. Thus, for short pulses and below $F_0 \leq 5\text{mJ}/\text{cm}^2$ the system is not demagnetised sufficiently to nucleate a large number of MD. At the same time, the topological protection is achieved with ultrafast cooling. For fluences larger than $F_0 > 7\text{mJ}/\text{cm}^2$ the energy deposited in the system is too high and the temperature fluctuations are too strong to allow stable MD and they merge into larger labyrinth-like domains. Further analysis and discussions are present in Supp. Mat. For pulses longer than 100fs, the system stays longer at high temperature and thermal activation is therefore

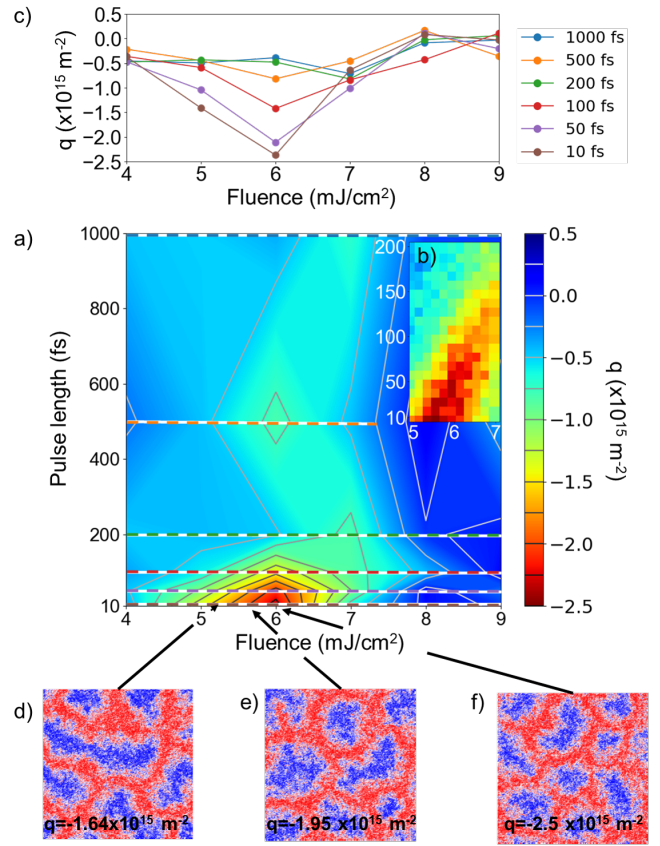


FIG. 3. (Color online) **Phase Diagram of skyrmion nucleation in zero external field.** a) Topological charge density q (color scale) as a function of laser fluence and pulse length. b) High resolution phase diagram showing the region with maximum topological density, averaged for 20 realisations; c) Topological charge density at selected pulse lengths as a function of fluence, the data correspond to the horizontal lines in panel a); Panels d), e), f) show examples of spin configurations for different topological charge densities;

more likely to lead the system to reach the ground state. Thus, the competition of different factors defines a unique window for laser parameters.

In the following we analyse the behaviour of the skyrmion lattice formation as a function of external magnetic fields applied in different orientations. Fig.4 shows the nucleation phase diagrams under several magnetic fields that are applied parallel ($B_{app} > 0$) or anti-parallel ($B_{app} < 0$) to the initial magnetisation direction. It is worth noting that in the presence of external fields of these magnitudes, skyrmion lattices are stable ground states of the system (See Supp. Mat.). Consequently, under long heating and subsequent cooling (for pulses longer than $t_p \geq 200\text{fs}$ and high fluences), the system reaches the skyrmion state. In this case either the intermediate paramagnetic state is achieved or the skyrmion nucleation process goes through thermal activation from the ferromagnetic state over the energy barrier in which

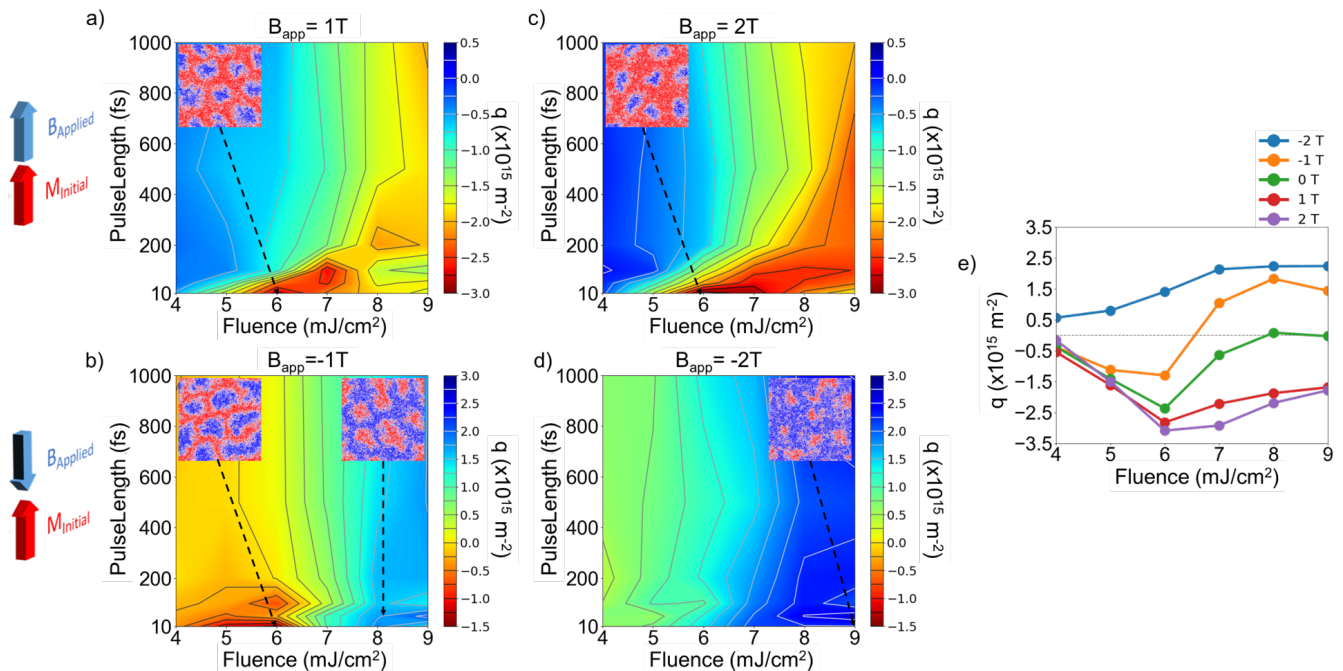


FIG. 4. (Color online) **Phase diagram when external fields are applied.** a) Phase Diagram when an external field of 1 Tesla is applied parallel to the initial magnetisation. b) Phase Diagram when an external field of 1 Tesla is applied antiparallel to the initial magnetisation. c) Phase Diagram when an external field of 2 Tesla is applied parallel to the initial magnetisation. d) Phase Diagram when an external field of 2 Tesla is applied antiparallel to the initial magnetisation. e) Topological charge density vs Laser fluence for selected external fields and for a fixed pulse width of 10 fs

case the deposited laser energy and its duration should be sufficient to achieve high reversal probability in order to reach a skyrmion state.

Focusing on shorter pulses (below $t_p < 200$ fs) for applied fields parallel to the initial magnetisation direction (Fig.4a and 4c) we observe that the region where skyrmion lattices are obtained is substantially increased for fluences $F_0 > F_C = 6 \text{ mJ/cm}^2$. This behaviour can be ascribed to the hindering of the growth of domains oriented antiparallel to the field. At the same time, once the skyrmion is created, an external field parallel to their core increases the energy barrier separating it from the other states [36] and the structure is more stable against fluctuations. The average topological charge densities are larger than those obtained in the zero-field case. This feature is in the first place related to the smaller skyrmion sizes due to the influence of external fields, allowing a large number of structures in the sample (see inset in Fig.4c). The effect of the applied field on the skyrmion size is investigated in the Supp. Mat. Importantly, there is a substantial influence of the non-equilibrium excitation. For example, in Fig.4a the region with fluences larger than $F_0 > 8 \text{ mJ/cm}^2$ and for $t_p < 200\text{fs}$ does not show the formation of the stable skyrmion lattice, while for less intense pulses skyrmion formation is obtained. This effect reveals once again that for pulses below $t_p < 200\text{fs}$ the system follows a non-equilibrium

excitation and the magnon localisation and coalescence processes take place.

Figs.4b and 4d show the nucleation phase diagrams for anti-parallel fields. Under an applied negative field, a ferromagnetic system can undergo ultrafast switching. In these cases, MD are nucleated with their core pointing parallel to the initial magnetisation. Thus, P-Sk lattices arise and the topological charge density carries a positive sign. This can be observed in Fig.4b and 4e (yellow line), where both positive and negative polarisations of skyrmion core can be obtained with field $B_{app} = -1\text{T}$ for short pulse lengths. Negative $q < 0$ values are consistent with the fact that larger fluences favor the magnetisation switching. For $B_{app} = -2\text{T}$, the Co trilayer magnetisation always switches its orientation. The effect of external fields is summarised in Fig.4e for a fixed ultrashort pulse width of $t_p = 50$ fs.

In conclusion we have modelled the linearly-polarised laser- (heat-)induced nucleation of skyrmion lattices in epitaxial cobalt-based asymmetric trilayers with perpendicular magnetic anisotropy. The system presents a ground state with labyrinth domains. The computed phase diagram for topological charge showed a nucleation window in terms of laser pulse intensity and duration, corresponding to ultra-fast lasers pulses shorter than $t_p < 200\text{fs}$. This shows the importance of highly thermodynamically non-equilibrium path for skyrmion

generation. This path involves magnon drop nucleation after the sample demagnetisation, and their topological protection during the magnon coalescence. Additionally, external fields enlarge the nucleation window, reduce skyrmion sizes and change the nucleation probability. Thus, we propose the important techniques and protocols to influence the desired skyrmion densities by a combined action of the laser pulse and external fields. Our results are important for the control of skyrmion nucleation for novel applications.

The authors acknowledge the networking opportunities provided by the European COST Action CA17123 "Magnetofon" and in particular the short-time scientific missions awarded to P.O.-R. and M.S. The work in Spain was supported by the Regional Government of Madrid through Project P2018/NMT-4321 (NANOMAGCOST-CM) and by the Spanish Ministry of Economy and Competitiveness (MINECO) through Projects SKYTRON (FIS2016-78591-C3-1-R and FIS2016-78591-C3-3-R) and FUNSOC (RTI2018-097895-B-C42). This project has received funding from the European Union's Horizon 2020 research and innovation programme under grant agreement No 737093 FEMTOTERABYTE and under the FLAG-ERA JTC2019 Project SOgraphMEM (MINECO PCI2019-111867-2). IMDEA Nanoscience Institute is supported by the "Severo Ochoa" Programme for Centres of Excellence in R&D, (MINECO grant SEV-2016-0686).

* pablo.olleros@imdea.org

† mss555@york.ac.uk

‡ paolo.perna@imdea.org

§ roy.chantrell@york.ac.uk

¶ oksana@icmm.csic.es

- [1] I. Dzyaloshinskii, *Sov. Phys. JETP* **5**, 1259 (1957).
- [2] T. Moriya, *Phys. Rev.* **120**, 91 (1960).
- [3] A. Fert, N. Reyren, and V. Cros, *Nature Mat.* **2**, 1 (2017).
- [4] R. Wiesendanger, *Nature Mat.* **1**, 16044 (2016).
- [5] S. Krause and R. Wiesendanger, *Nature Mater.* **15**, 493 (2016).
- [6] J. Sampaio, V. Cros, S. Rohart, A. Thiaville, and A. Fert, *Nature Nanotechnol.* **8**, 839 (2013).
- [7] Y. Huang, W. Kang, X. Zhang, Y. Zhou, and W. Zhao, *Nanotechnology*. **28**, 08LT02 (2017).
- [8] G. Bourianoff, D. Pinna, M. Sitte, and K. Everschor-Sitte, *AIP Adv.* **8**, 055602 (2018).
- [9] C. Moreau-Luchaire, C. Moutafis, N. Reyren, J. Sampaio, C. Vaz, N. Van Horne, K. Bouzehouane, K. Garcia, C. Deranlot, P. Warnicke, *et al.*, *Nature nanotechnology* **11**, 444 (2016).
- [10] S. Woo, K. Litzius, B. Krüger, M.-Y. Im, L. Caretta, K. Richter, M. Mann, A. Krone, R. Reeve, M. Weigand, P. Agrawal, I. Limesh, M.-A. Mawass, P. Fischer, M. Klaui, and G. Beach, *Nature Mat.* **15**, 501 (2016).
- [11] W. Jiang, W. Upadhyaya, Pand Zhang, M. Yu G.and Jungfleisch, F. Fradin, Y. Pearson, JE and; Tserkovnyak, K. Wang, O. Heinonen, S. te Velthuis, and A. Hoffmann, *Science* **349**, 283 (2015).
- [12] S. Finizio, K. Zeissler, S. Wintz, S. Mayr, T. Weßels, A. J. Huxtable, G. Burnell, C. H. Marrows, and J. Raabe, *Nano letters* **19**, 7246 (2019).
- [13] A. Kirilyuk, A. Kimel, and T. Rasing, *Rev.Mod. Phys.* **82**, 2731 (2010).
- [14] R. Ostler, J. Barker, R. Evans, R. Chantrell, U. U. Atxitia, O. Chubykalo-Fesenko, S. El Moussaoui, L. Le Guyader, E. Mengotti, L. Heyderman, F. Nolting, A. Tsukamoto, A. Itoh, D. Afanasiev, B. Ivanov, A. Kalashnikova, K. Vahaplar, J. Mentink, A. Kirilyuk, T. Rasing, and A. Kimel, *Nature Comm.* **3**, 666 (2012).
- [15] S.-G. Je, P. Vallobra, T. Srivastava, J.-C. Rojas-Sánchez, T. H. Pham, M. Hehn, G. Malinowski, C. Baraduc, S. Auffret, G. Gaudin, *et al.*, *Nano Lett.* **18**, 7362 (2018).
- [16] M. Finazzi, M. Savoini, A. Khorsand, A. Tsukamoto, A. Itoh, L. Duò, A. Kirilyuk, T. Rasing, and M. Ezawa, *Physical review letters* **110**, 177205 (2013).
- [17] R. Moreno, R. Evans, S. Khmelevskiy, M. Muñoz, R. Chantrell, and O. Chubykalo-Fesenko, *Phys. Rev. B* **94**, 104433 (2016).
- [18] H. Yang, A. Thiaville, S. Rohart, A. Fert, and M. Chshiev, *Phys. Rev. Lett* **115**, 267210 (2015).
- [19] O. Boule, J. Vogel, H. Yang, S. Pizzini, D. de Souza Chaves, A. Locatelli, T. O. Menteş, A. Sala, L. D. Buda-Prejbeanu, O. Klein, *et al.*, *Nature Nanotechnol* **11**, 449 (2016).
- [20] J. Barker, U. Atxitia, T. Ostler, O. Hovorka, O. Chubykalo-Fesenko, and R. Chantrell, *Sci.Rep.* **3**, 3262 (2013).
- [21] E. Iacocca, T.-M. Liu, A. Reid, Z. Fu, S. Ruta, P. Granitzka, E. Jal, S. Bonetti, A. Gray, C. Graves, *et al.*, *Nature Comm.* **10**, 1 (2019).
- [22] R. F. Evans, W. J. Fan, P. Churemart, T. A. Ostler, M. O. Ellis, and R. W. Chantrell, *Journal of Phys.: Cond. Mat.* **26**, 103202 (2014).
- [23] F. Ajejas, V. Křížáková, D. de Souza Chaves, J. Vogel, P. Perna, R. Guerrero, A. Gudín, J. Camarero, and S. Pizzini, *Applied Physics Letters* **111**, 202402 (2017).
- [24] F. Ajejas, A. Gudín, R. Guerrero, A. Anadón Barcelona, J. M. Diez, L. de Melo Costa, P. Olleros, M. A. Niño, S. Pizzini, J. Vogel, *et al.*, *Nano letters* **18**, 5364 (2018).
- [25] P. Olleros-Rodríguez, R. Guerrero, J. Camarero, O. Chubykalo-Fesenko, and P. Perna, *ACS Applied Materials & Interfaces* (2020).
- [26] L. Jiang and H.-L. Tsai, *J. of Heat Transf.* **127**, 1167 (2005).
- [27] P. Metaxas, J. Jamet, A. Mougin, M. Cormier, J. Ferré, V. Baltz, B. Rodmacq, B. Dieny, and R. Stamps, *Phys. Rev. Lett.* **99**, 217208 (2007).
- [28] R. Chimata, A. Bergman, L. Bergqvist, B. Sanyal, and O. Eriksson, *Phys. Rev. Lett.* **109**, 157201 (2012).
- [29] J.-Y. Bigot, M. Vomir, L. Andrade, and E. Beaupaire, *Chem. Phys.* **318**, 137 (2005).
- [30] W. Koshibae and N. Nagaosa, *Nature communications* **5**, 1 (2014).
- [31] S. Lepadatu, Emergence of transient domain wall skyrmions after ultrafast demagnetisation (2020), arXiv:2005.13238 [cond-mat.mes-hall].
- [32] L. Rózsa, E. Simon, K. Palotás, L. Udvardi, and L. Szunyogh, *Phys. Rev. B* **93**, 024417 (2016).
- [33] N. Kazantseva, U. Nowak, R. W. Chantrell, J. Hohlfeld, and A. Rebei, *EPL (Europhys. Lett.)* **81**, 27004 (2007).
- [34] E. Turgut, D. Zusin, D. Legut, K. Carva, R. Knut, J. M.

- Shaw, C. Chen, Z. Tao, H. T. Nembach, T. J. Silva, *et al.*, Phys. Rev. B **94**, 220408 (2016).
- [35] M. Maiden, L. Bookman, and M. Hofer, Phys. Rev. B **89**, 180409 (2014).
- [36] F. Tejo, A. Riveros, J. Escrig, K. Guslienko, and O. Chubykalo-Fesenko, Sci. Rep. **8**, 1 (2018).